Modelling microstructural evolution and mechanical properties of austempered ductile iron

R. C. Thomson, J. S. James, and D. C. Putman

Austempered ductile iron (ADI) is finding an ever increasing worldwide market in the automotive and other sectors. It offers a range of mechanical properties superior to those of other cast irons, and shows excellent economic competitiveness with steels and aluminium alloys. The aim of the present research is to develop a generic model that will enable the producers of ADI to optimise their product in terms of microstructure and mechanical properties, hence minimising the need for expensive and exhaustive experimental trials and reducing alloy development lead times.

MST/4800

At the time the work was carried out, the authors were at the Institute of Polymer Technology and Materials Engineering, Loughborough University, Loughborough, Leicestershire LE11 3TU, UK. Dr James is now at Federal–Mogul Technology, Cawston, Rugby, Warwickshire CV22 7SA, UK. *Contribution to the 'Structure of materials' section of Materials Congress 2000 organised by IoM at Cirencester on 12–14 April 2000.*

Introduction

A wide range of properties can be obtained in austempered ductile iron (ADI) components owing to changes in the proportions of the major phases present in the microstructure: bainitic ferrite, high carbon austenite, and graphite nodules. Martensite, ferrite, iron carbides, and other alloy carbides may also be present. A considerable amount of work on the relationship between the composition, heat treatment, microstructure, and properties of ADI has been reported (for example, *see* Refs. 1 and 2). However, there appears to be little reference to modelling to enable prediction of the differing microstructures possible in ADI, which is the focus of this research. The present paper describes a generic model that can predict the amounts of the major phases present in the microstructure, and the transformation kinetics of the austempering reaction as a function of composition and heat treatment parameters using fundamental thermodynamic and kinetic theory, and additionally demonstrates how this can be used to predict simple mechanical properties such as strength.

The microstructure is dependent on both the composition of the cast iron and the exact parameters of the four stages in the production process. The process comprises the production of a ductile iron casting, austenitisation (at about 800–950°C), subsequent quenching to a temperature (about 250–400°C) suitable for the final stage, and the isothermal transformation (austempering) of some of the austenitic matrix to other phases before subsequent cooling to room temperature. The austempering heat treatment, in addition to the austenitisation heat treatment, is of significance in determining the exact microstructure produced, and can itself be considered to occur in a series of stages. In the first stage of the austempering process, the metastable austenite will transform into a mixture of bainitic ferrite and high carbon austenite. The exact temperature employed in the austempering process will affect the structure of the bainitic ferrite: at the higher austempering temperatures within the range the bainite will be carbide free (cf. upper bainite in steels), whereas at the lower temperatures the bainite transformation may be accompanied by carbide precipitation (cf. lower bainite in steels), resulting in a mixture of bainitic ferrite, carbide, and high carbon austenite. The high carbon austenite will eventually decompose into a mixture of thermodynamically more stable ferrite and carbide on prolonged heat treatment; this is termed the stage II reaction. Hence, there is a well defined processing window[2] during which a relatively stable structure of bainitic ferrite and high carbon austenite, often termed ausferrite, exists between the stage I and stage II reactions. The addition of alloying elements can greatly affect the thermodynamics and kinetics of the phase transformations, and the segregation present within the cast iron, and therefore the processing window will change as a function of alloy content, resulting in overlaps between the two stages and potential closure of the processing window.

The present model concentrates on predicting the changes that occur during stage I (Ref. 2) of the austempering process. It has also been assumed that the high silicon content present in ADI will largely prevent the formation of carbide during the stage I reaction at the lower austempering temperatures, and therefore any carbide formation accompanying the bainite reaction has not been taken into consideration. The development of a quantitative model that allows for the precipitation of carbides accompanying the bainite transformation remains one of the challenges in phase transformation theory.[3] Predictions are therefore realistic for commercial alloys which are heat treated within a processing window before significant onset of the stage II reaction.

Austenitisation

After the initial production of a ductile iron casting to near net shape for a particular component, it then undergoes heat treatment first involving an austenitisation treatment at temperatures typically between 850 and 950°C. The temperature and time of this austenitisation step are critical in determining the carbon content of the austenite matrix for subsequent isothermal transformation at lower temperatures. The high temperature equilibrium between graphite and austenite has been investigated using thermodynamic modelling techniques. The equilibrium austenite carbon content and the volume fraction of graphite at the austenitisation temperature were determined by Gibbs energy minimisation calculations performed using

 ISSN 0267–0836

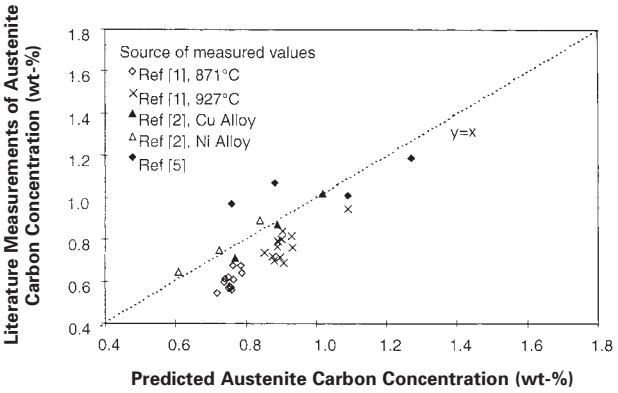

1 Equilibrium carbon content in austenite predicted using MTDATA[4] with SGTE database compared with measured values reported in literature[1,2,5] for variety of austempered ductile iron compositions and austenitising temperatures, and austenitising times >60 min: line *y*=*x* represents perfect agreement between predicted and measured values

MTDATA[4] and the SGTE (Scientific Group Thermodata Europe) database. Extensive checks were performed on the accuracy of such calculations by comparison of the calculated austenite carbon content with measured values from the literature for austenitising times greater than 60 min, for which a state close to equilibrium could be expected to have been attained (*see* Fig. 1). The cast irons used in these calculations contained a variety of different elements. Those heat treated at 871 and 927° (Ref. 1) comprised ~3·6 wt-%C and 2·5 wt-%Si with additions of up to 1 wt-%Mn, 0·6 wt-%Mo, and 1·5 wt-%Ni added both individually and synergistically; the copper containing alloy[2] was ~3·8 wt-%C, 2·8 wt-%Si with 0·3 wt-%Cu; the nickel containing alloy[2] was ~3·6 wt-%C, 2·8 wt-%Si with 1 wt-%Ni; the remaining alloy[5] had a higher carbon content at ~4·2 wt-%C with 2·9 wt-%Si and 0·3 wt-%Mn. The carbon concentrations were determined by X-ray diffraction[1,2] and an indirect method based on the start temperature of the martensite reaction.[5] Hence, a representative spread of compositions used for commercial cast irons was used for comparison of the measured and predicted carbon concentrations in austenite, and reasonable agreement was observed.

Measurements were also made of the graphite volume fraction using image analysis techniques for cast irons of several different compositions and austenitisation conditions,[6] and were found to be in good agreement with predicted values. Having validated the accuracy of the austenite–graphite equilibrium at typical austenitising temperatures, it was also possible to perform 'thought' experiments to investigate the effect of typical alloying elements on the austenite carbon content. The results from such calculations are presented in Fig. 2, in which the percentage change in equilibrium austenite carbon content is plotted as a function of the relative change in the concentration of each alloying element in isolation. The base composition of the cast iron used for the calculations was Fe–3·66C–2·52Si–0·16Mn–0·04P–0·01S–0·03Cr–0·51Cu–0·04Mg (wt-%). It should be noted that a small percentage change in the austenite carbon content can have a significant effect on the subsequent austempering reaction, changing the volume fraction of the phases present and, hence, the resulting mechanical properties. From Fig. 2 it can be seen that the elements predicted to have the most effect are silicon and copper, hence giving an indication to the foundry regarding which elements should be controlled most tightly within alloy composition specifications.

It is clear, however, that during the austenitisation heat treatment some time will be necessary before equilibrium has been obtained, and therefore modelling of the austenitisation process must be able to consider a range of possible austenitising times. Darwish and Elliott[2] showed that for a cast iron of composition Fe–3·80C–2·77Si–0·037Mn–0·03P–0·02S–0·02Cr–0·07Ni–0·33Cu–0·034Mg (wt-%) the austenite carbon content increased gradually up to a constant value over a period of ~20 min at 1000°C and 70 min at 850°C. The austenite carbon content for short austenitising times (times up to 50 min) can be calculated using an empirical relationship (for a particular composition) derived from the above results. More rigorous calculations have been carried out to model the austenitisation process using a diffusional approach, capable of including composition and segregation effects for any composition.[5] The times calculated for the carbon concentration to equilibrate are in agreement with measured values, and calculations demonstrate that during the austempering heat treatment in specimens which have been initially given very short austenitising times, bainite is found only in regions closest to the graphite nodules as the initial 'bull's eye' ferritic–pearlitic structure transforms to austenite over finite time periods.

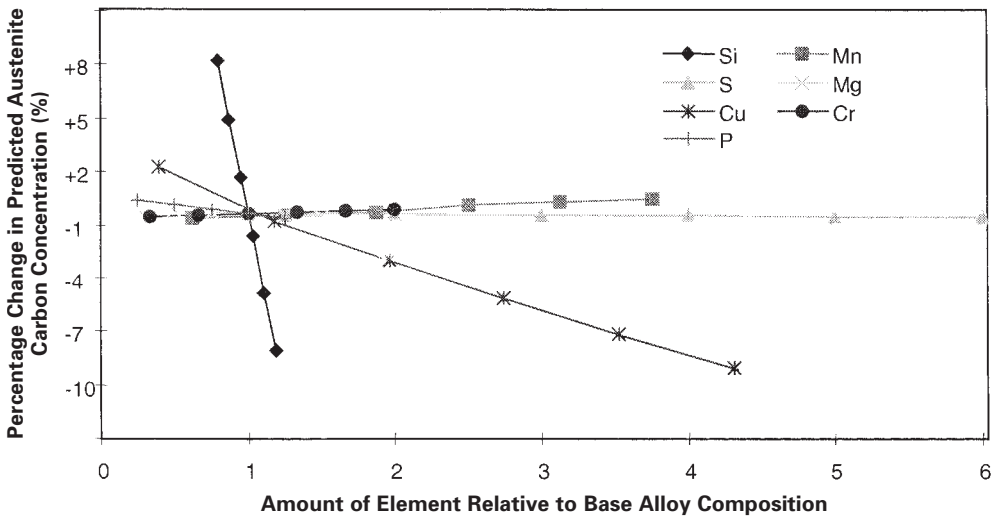

2 Calculations showing effect of varying alloying element concentration with respect to base alloy composition on predicted amount of carbon in austenite

Having obtained the carbon content in austenite and the volume fraction of graphite at the austenitising temperature, it was assumed that neither changed significantly during subsequent quenching to the austempering temperature.

Austempering

VOLUME FRACTION OF BAINITIC FERRITE

Following quenching from austenite, the transformation of supersaturated austenite to bainitic ferrite is carried out isothermally. In a model proposed for steels[7,8] and modified by the present authors for ADI, supersaturated austenite transforms to supersaturated bainitic ferrite via a displacive mechanism. Following the transformation, carbon diffuses from the bainitic ferrite to the remaining austenite. This leads to an increase in the austenite carbon content and, hence, to a reduction in the Gibbs energy difference between the two phases, the driving force for the reaction. The diffusionless transformation ceases when the driving force reaches zero, leading to the 'incomplete reaction phenomenon'. The maximum carbon content at which the transformation can occur x_{T_0} increases with decreasing austempering temperature. Calculation of this carbon content can be carried out for a limited number of elements using carbon activity data,[9] or for all elements of interest by determination of free energies of austenite and ferrite at the appropriate temperature using MTDATA.[4]

Measurements of the untransformed austenite volume[10] and the volume fraction of bainitic ferrite[8] indicate that the reaction ceases at, or close to, x_{T_0} in both ADI and steels, rather than $x_{T_0'}$, the limiting carbon content when the strain energy associated with the transformation ($\sim$400 J mol^{-1} in steels[9]) is taken into account. It was found in the present research that there was better agreement between predictions of the volume fraction of bainitic ferrite and measurements made experimentally using dilatometric techniques, than proportions reported in the literature determined from X-ray diffraction experiments. A possible explanation for this[9,11] is that the heterogeneous distribution of carbon in austenite results in lower carbon regions potentially decomposing to martensite on subsequent cooling. Therefore, carbon concentrations determined from the lattice parameter of retained austenite may be artificially high, resulting in an overestimation of the volume fraction of bainitic ferrite. Hence, in the present research a modified value for the carbon content at which the bainite reaction ceases x_{T^*} was used, which better represents agreement between the model predictions and values of bainite volume fraction quoted in the literature for austempered ductile irons. Numerically, the use of x_{T^*} resulted in carbon contents slightly higher than x_{T_0} and closer to values determined from growth rates in low alloy steels reported by Hillert.[12] The dependence on temperature of this value for the carbon concentration at which the bainite reaction ceases was assumed to be linear; however, this should be the subject of future investigations.

The maximum volume fraction of bainitic ferrite V_b can then be calculated for the alloy composition of interest using the lever rule

$$V_b = \frac{x_{T^*} - x_\gamma}{x_{T^*} - x_\alpha} \quad . . . . . (1)$$

The matrix carbon content x_γ is taken as the value determined from the calculation of the austenite–graphite equilibrium at the austenitising temperature, and the carbon content of the (saturated) ferrite x_α is calculated at the austempering temperature using a polynomial expression derived from empirical data.[13] The results of the lever rule calculation have been compared with measurements, both those made by the present authors and other values reported in the literature, of the volume fraction of bainitic ferrite for various alloys and heat treatment parameters (*see* Fig. 3).

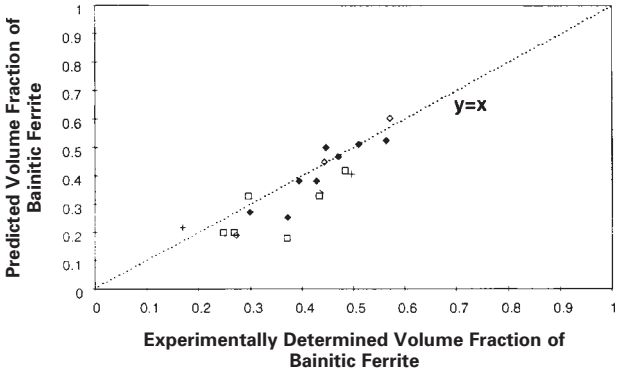

3 Comparison of experimental measurements of volume fraction of bainitic ferrite using variety of methods[5] and predictions using microstructural model for variety of austempered ductile iron compositions, austenitising and austempering temperatures, and times

TRANSFORMATION KINETICS

A model developed for low alloy steels[7,8] was modified to allow predictions of the transformation kinetics of the bainite reaction for the higher concentrations of certain alloying elements found in austempered ductile irons. The amount of bainite is expressed as a normalised volume fraction ξ, which is the maximum possible volume fraction V_b determined from the limiting carbon concentration, as described above, divided by the total volume. The increase in the normalised volume fraction $d\xi$ in time dt is then given by

$$V_b \, d\xi = (1-\xi) u I \, dt \quad . . . . . (2)$$

where u is the volume of a bainite 'subunit' and I is the nucleation rate per unit volume. The nucleation rate I is a function of the temperature and the maximum free energy available for the nucleation of ferrite ΔG_{max}

$$I = K_1 \exp\left(-\frac{K_1}{RT} - \frac{K_2 \Delta G_{max}}{rRT}\right) \quad . . . . . (3)$$

where r, K_1 and K_2 are constants, T is the temperature, and R is the universal gas constant. The value of ΔG_{max} is in turn affected by the original composition of the cast iron and enrichment of the austenite with carbon as the reaction proceeds. The free energy available for nucleation has been assumed to vary linearly between an initial value ΔG^0_{max} determined at the original carbon content (equal to the final carbon content of the matrix after austenitisation) and the limiting free energy change when nucleation ceases, the universal nucleation function G_N

$$\Delta G_{max} = \Delta G^0_{max} - \xi(\Delta G^0_{max} - G_N) \quad . . . . . (4)$$

Solution of equations (2), (3), and (4) (Ref. 8) hence yields the transformation kinetics of the bainite reaction, allowing calculation of the increase in volume fraction of bainite with time at the austempering temperature. It was necessary, however, to determine new values for one of the fitted constants in the original model[8] to account for the significant differences in alloy composition between austempered ductile irons and low alloy steels. A new function for the autocatalysis term β, which describes the increased rate of nucleation in austenite adjacent to previously formed bainitic ferrite, was introduced.[14] The original relationship $\beta = \lambda_1(1-\lambda_2 x)$ was modified to vary according to the relationship $\beta_m = \lambda_1/\exp(2\lambda_2 x)$, where λ_1 and λ_2 are

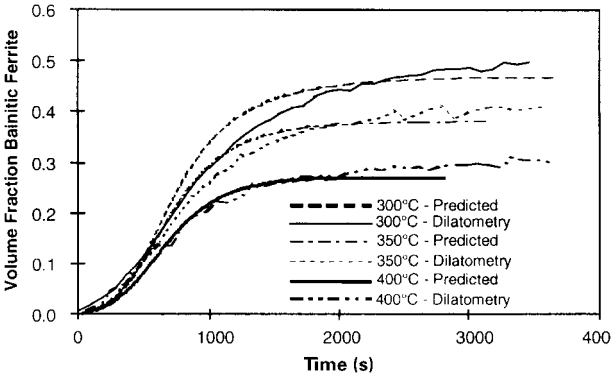

4 Predicted curves for transformation to bainitic ferrite during austempering at 300, 350, and 400°C compared with experimental measurements made using dilatometry[5]

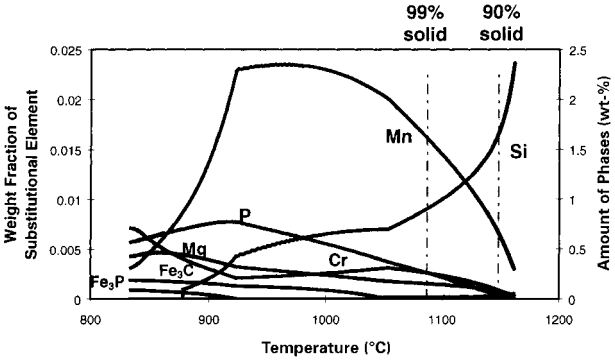

5 Predicted segregation profile of substitutional elements using Scheil approach to solidification: decrease in temperature corresponds to increase in amount of solid formed on cooling

optimised empirical constants and x is the mean (matrix) carbon content, hence resulting in a value for β which remains positive at all carbon contents but drops off to a low value at the higher carbon concentrations.

Figure 4 shows the predicted rate of transformation for a cast iron of composition Fe–3·66C–2·52Si–0·16Mn–0·04P–0·01S–0·03Cr–0·51Cu–0·04Mg (wt-%) at three austempering temperatures, 300, 350, and 400°C, together with the experimentally determined rates using dilatometric techniques. All three specimens, 8 mm in diameter and 12 mm in length, were initially homogenised for 3 days at 1000°C and then were given an austenitisation treatment for 15 min at 950°C before austempering. It can be seen that there is reasonable agreement between the predicted and measured bainite transformation curves, particularly with respect to the initial transformation kinetics, although there is a small difference between the predicted and measured final volume fraction of bainitic ferrite. It should be noted that any carbide precipitation accompanying the transformation to bainitic ferrite at the lower austempering temperatures has not been taken into account in modelling of the transformation kinetics. Nevertheless, the model is capable of estimating the length of the austempering treatment necessary to permit the maximum possible volume fraction of bainite to form within the microstructure of ADI.

Chemical segregation

The fact that ADI originates from a cast microstructure means that chemical segregation present within a casting must also be taken into account. As the initial casting is cooled below the eutectic temperature, graphite and austenite grow simultaneously as a divorced eutectic, with the austenite forming in shells surrounding the graphite. Growth of the graphite proceeds by diffusion of carbon through the austenite. Thus, the first regions to solidify contain the graphite nodules and the last regions to solidify are those remote from the nodules. As freezing progresses, solute atoms partition between the solid and liquid so that the composition of the solid changes and a chemical segregation profile is produced.

This chemical segregation can be represented by the classical 'Scheil' equation in which it is assumed that there is local equilibrium at the solid/liquid interface, with complete mixing in the liquid state and no backdiffusion of elements in the solid state. It should be noted that in steels this assumption is known to produce erroneous results as carbon diffuses rapidly in austenite; however, for the eutectic transformation in cast irons graphite and austenite are in equilibrium and, therefore, Scheil calculations can be expected to give reasonable predictions for the substitutional element distribution.[15] Carbon will also redistribute rapidly during the subsequent high temperature austenitisation treatment. Calculations were carried out using the Scheil macro within MTDATA to perform Gibbs energy minimisations between liquid and solid phases over a range of decreasing temperatures.

The results of the Scheil calculations are presented in Fig. 5. It can be seen that there is a strong tendency for silicon to partition to the solid and manganese to the liquid, resulting in high concentrations of manganese and correspondingly low concentrations of silicon being found in the last liquid to solidify, i.e. in a region halfway between two graphite nodules. These predicted segregation tendencies agree well with those reported in the literature;[16–21] however, the solidification pattern is complex and direct comparison between modelling and experimental results is non-trivial. Molybdenum, also an extremely important element from hardenability considerations,[22–25] was not present in the cast iron considered in the present calculations; however, in alloys of appropriate composition it has been demonstrated that it too partitions to the liquid, behaving in a similar manner to manganese. The calculations also show that small quantities of carbides and phosphides, Fe_3C and Fe_3P respectively, are predicted to occur in the last liquid to solidify. Particles containing high levels of iron, manganese, and phosphorus have been identified using energy dispersive X-ray analysis in the scanning electron microscope, in regions approximately halfway between two graphite nodules[5] (*see* Fig. 6).

It is possible by using Scheil calculations to build up a series of shells, each of different chemical composition, representing sequential regions adjacent to the graphite nodules progressing towards the last liquid to solidify, halfway between two nodules. One particular problem encountered is that the Scheil simulation predicts the formation of graphite, ostensibly, within each shell, the amount of which depends on the solubility of carbon in the austenite. This distribution of graphite throughout the shells persists into the modelling of the austenitisation, during which growth or dissolution of graphite nodules is represented by an increase or decrease of the amount of graphite in each shell. The sum of the amount of graphite in the individual shells is equivalent to that in the whole of the graphite nodule(s). This distribution of graphite among the shells is an artefact of the Scheil type simulation, produced by the assumption of zero carbon diffusivity in the solid. The distribution of graphite throughout the shells also persists into the modelling of austempering. The presence of graphite in the shells has no bearing on the proportion of the austenite that transforms to bainitic ferrite in the

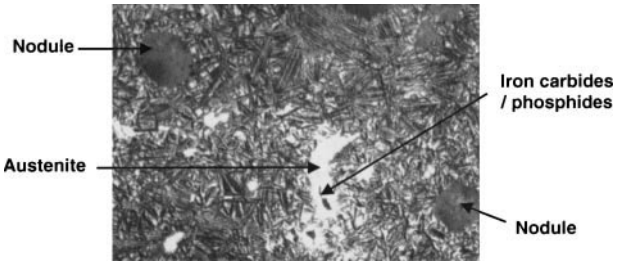

6 Optical micrograph illustrating formation of primary carbides/phosphides in last liquid to solidify, approximately halfway between graphite nodules, and reduced amount of bainitic ferrite in same region owing to chemical segregation within microstructure

individual shells. This is determined by the austenite carbon content, which is, in turn, dependent on the solubility of carbon as a function of substitutional element concentrations. However, the presence of graphite in each shell reduces the amount of austenite 'available' for transformation, and therefore the predicted amount of bainitic ferrite must be scaled to account for this. Hence, the effect of segregation due to the casting process on subsequent austempering can be deduced.

Using the compositions predicted to occur within each individual shell of material from the Scheil model for solidification, and following the procedures described above for the prediction of the volume fraction of bainite formed as a function of austenitising and austempering temperatures and times, it was possible to investigate the effect of chemical inhomogeneity on the heat treated microstructure. The results from calculations for a cast iron of composition Fe–3·72C–2·02Si–0·44Mn–0·03P–0·01S–0·05Cr–0·01Ni–0·04Cu–0·051Mg (wt-%) are presented in Fig. 7. The values of x_γ, the calculated carbon content in austenite at the end of the austenitisation heat treatment (assumed to have reached equilibrium) for austenitisations at 850 and 950°C, and x_{T_0}, the limiting carbon concentration calculated from the free energy curves of austenite and ferrite at a particular austempering temperature (250 and 350°C), for the individual shells are shown in Fig. 7*a*. It can be seen that as the distance from the graphite nodule increases, x_γ increases and x_{T_0} decreases and, hence, a lower maximum volume fraction of bainitic ferrite is predicted in material remote from the nodules after austempering, shown in Fig. 7*b*. Indeed, for the 950°C plus 350°C heat treatment no bainite at all is predicted to occur in such regions. This prediction of a reduced amount of bainite in regions approximately halfway between the nodules is consistent with the observed microstructure (*see* Fig. 6 for the microstructure of the cast iron with the same composition as that used for the calculations in Fig. 7 after austenitisation at 850°C and austempering at 350°C both for 60 min).

It was determined from these calculations that the presence of chemical segregation results in a slightly smaller overall volume fraction of bainite in the microstructure than would be expected if the specimen were homogeneous. Scheil calculations, linked with the prediction of phase transformations, have therefore been demonstrated to be useful and representative of a number of observed microstructural features, in particular the presence of carbides/phosphides and very little bainite in regions representative of the last liquid to solidify, approximately halfway between graphite nodules.

Combined model

It has been demonstrated above how the volume fraction of graphite is obtained from calculation of the austenite–graphite equilibrium at the austenitising temperature, and that the volume fraction of bainite can be obtained from a lever rule calculation based on a model developed for low alloy steels. The amount of other major phase in the microstructure, high carbon austenite, was calculated by assuming that the remaining microstructure at the end of austempering, but before final cooling to ambient temperatures, consisted of austenite. It was further assumed that a proportion of this austenite would transform to martensite dependent on the M_s temperature, i.e the start temperature of the martensite reaction for the alloy composition of interest. The M_s temperature was determined using the expression proposed by Andrews[26] in which the austenite carbon content is assumed to be that at the point when transformation to bainite ceases corresponding to the end of the austempering process, x_{T*}. Hence, the volume fraction of martensite could be determined from knowledge of the M_s temperature and the final quenching temperature, assumed to be room temperature.

A schematic diagram summarising the various components of the overall microstructural model for ADI is presented in Fig. 8. Figure 9 illustrates a typical set of predictions of the major phases in the final microstructure in

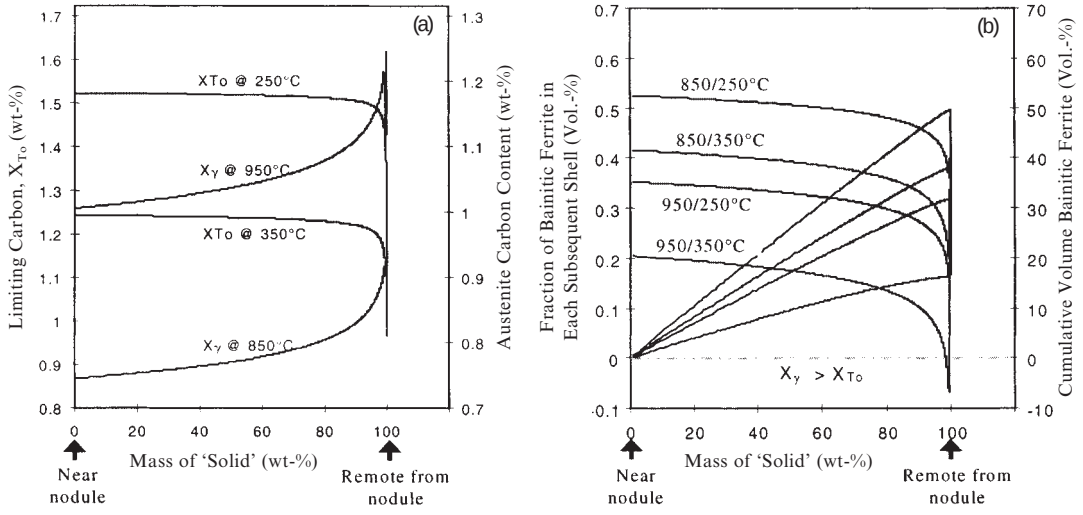

a austenite C content at start of austempering and limiting C content; *b* volume fraction of bainite within segregated matrix

7 Determination of amount of bainitic ferritic as function of position within segregated matrix for four different heat treatment conditions

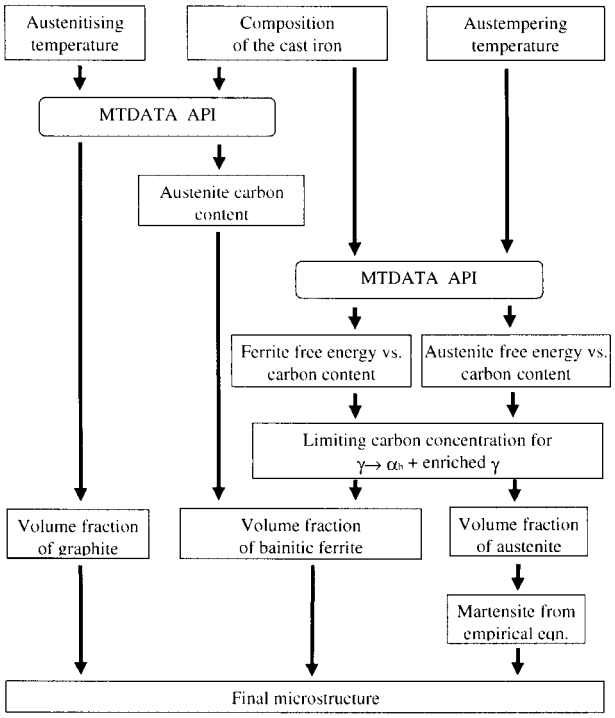

8 Structure of combined model using MTDATA application interface for prediction of overall microstructure of austempered ductile iron (ADI) castings

an austempered ductile iron with an initial composition Fe – 3·72C – 2·02Si – 0·44 Mn – 0·035P – 0·007S – 0·01Ni – 0·04Cu – 0·051Mg (wt-%) as a result of four different heat treatment processes. It should be noted that the austempering temperature has a greater effect on the proportions of phases within the microstructure than the austenitising temperature, as expected. Figure 10 additionally provides a comparison of the predicted amounts of austenite present in the microstructure and measured volume fractions for a range of cast irons available in the literature.

Mechanical properties

The ultimate goal of microstructure modelling methodologies is to be able to relate the predicted microstructure to mechanical properties, hence allowing alloy design by

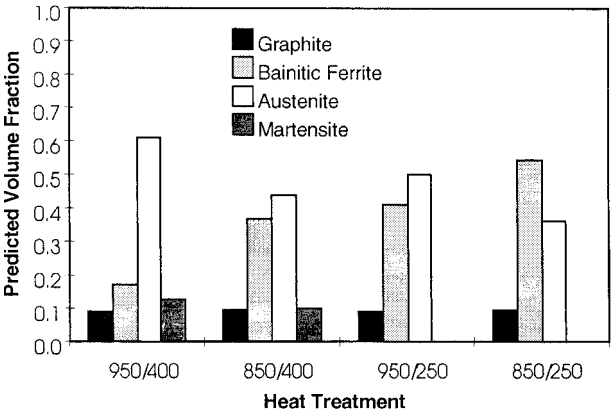

9 Example prediction using microstructural model of major phases in ADI: *x* axis scale gives austenitisation and austempering temperatures (°C), with both heat treatments being carried out for 60 min

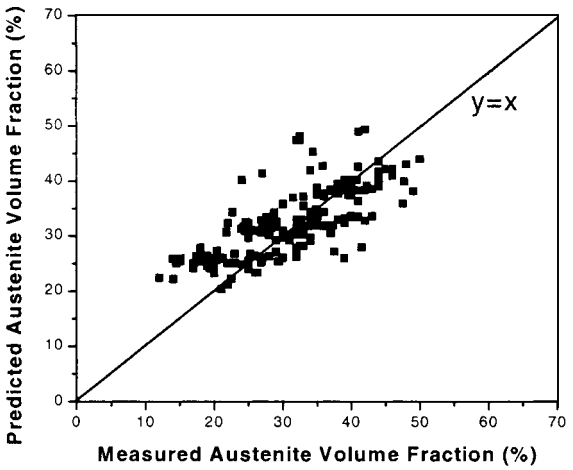

10 Comparison of predicted austenite volume fractions and experimental values reported in literature for variety of ductile iron compositions and austenitising temperatures and times

computer to produce components with the desired performance. Properties of particular interest for ADI components include tensile strength, hardness, fatigue, ductility, toughness, and wear resistance.

To develop a model for the yield strength of ADI as a function of the volume fraction of the phases present in the microstructure, a simple law of mixtures approach was assumed to be valid as a first approximation, i.e. that each phase contributes proportionally to the overall strength weighted by volume fraction. It was therefore necessary to develop models for the strength of each of the individual components within the microstructure.

BAINITE AND MARTENSITE

The strength of bainite and martensite can be factorised into a number of components:[27,28]

(i) strength of pure annealed iron
(ii) solid solution strengthening
(iii) interstitial carbon strengthening
(iv) strengthening due to lath size
(v) strengthening due to dislocations.

Pure body centred cubic iron has a lattice strength of 219 MPa at room temperature. Substitutional solutes do not partition during the displacive growth of either bainite or martensite, and therefore their concentrations are determined by the bulk composition. There are a number of models in the literature for the contribution to strength from a variety of elements in solid solution, all with varying degrees of accuracy. Therefore, in the present work the contributions of individual elements were largely estimated as a function of temperature and strain rate from published experimental data.[29] Bainite has a very low solubility for carbon at ~0·02 wt-%, whereas martensite forms from enriched austenite and can therefore contain much higher carbon levels. In the present work the carbon content of any martensite that formed was taken as the carbon content of the austenite at the end of the austempering process, as predicted by the microstructural model. Solid solution theory indicates that the strength due to dissolved carbon should vary with the square root of the carbon concentration. The contribution to the strength of bainite[30] σ_{ss} resulting from dissolved carbon is given by

$$\sigma_{ss} = 1722{\cdot}5x^{1/2} \quad . . . . . (5)$$

and that for martensite[31] by

$$\sigma_{ss} = 1171{\cdot}3x^{1/3} \quad . . . . . (6)$$

where the strength is in MPa, and the concentration of carbon x is expressed in wt-%.

The shape change resulting from shear transformation during the formation of martensite or bainite causes plastic deformation and, hence, the accumulation of dislocations in the parent and product phases. The extent of the plasticity depends on the yield strength and, hence, on temperature. It has been suggested that the dislocation density ρ_d can be represented empirically as a function of temperature alone for the temperature range 570–920 K (Ref. 32)

$$\log_{10}(\rho_d) = 9{\cdot}2840 + \frac{6880{\cdot}73}{T} - \frac{1\,780\,360}{T^2} \quad . \; . \; . \quad (7)$$

where T is the transformation temperature in K and ρ_d is stated in units of m^{-2}. The strengthening of bainite σ_ρ (MPa) due to the dislocations is given by

$$\sigma_\rho = 0{\cdot}38\mu b(\rho_d)^{0{\cdot}5} \approx 7{\cdot}34 \times 10^6(\rho_d)^{0{\cdot}5} \quad . \; . \; . \; . \; . \; . \; . \; . \; . \; . \quad (8)$$

where μ is the shear modulus and b is the magnitude of the Burgers vector.

Martensite and bainite grow as very fine plates or laths. These laths or plates contribute a grain size strengthening σ_g to the overall strength of the steel, defined as[27]

$$\sigma_g = 115(\bar{L})^{-1} \quad . \; . \; . \; . \; . \; . \; . \; . \; . \; . \; . \; . \; . \quad (9)$$

where σ_g is in MPa, and $\bar{L}$ is is the mean linear intercept measured on random sections and is approximately twice the plate size. It is clear that the bainitic ferrite plate size changes with austempering temperature, and therefore an empirical relationship was derived from measurements made from transmission electron micrographs that expressed plate size as a function of temperature. A typical value for the bainitic ferrite plate size at an austempering temperature of 350°C was ~0·6 μm. The martensite plate size was assumed to be half that of the bainitic ferrite as a first approximation; little or no martensite was predicted to form in the majority of the alloys of interest.

For an alloy of composition Fe–3·49C–2·33Si–0·42Mn–0·004P–0·016S–0·23Mo–0·25Cu–0·035Mg (wt-%) austempered at 350°C, the contributions to the strength were as follows: iron 219 MPa, carbon 244 MPa, solid solution elements 250 MPa, plate size 92 MPa, and dislocations 547 MPa, giving an overall strength of 1352 MPa, which is not unreasonable for a fully bainitic microstructure.

AUSTENITE

Calculation of the austenite strength σ_y was based on an empirical equation from the work of Singh and Bhadeshia[33] on low alloy steels

$$\begin{aligned}\sigma_y\ (\text{MPa}) = {} & [1 - (0{\cdot}26 \times 10^{-2})T_r \\ & + (0{\cdot}47 \times 10^{-5})T_r^2 \\ & - (0{\cdot}326 \times 10^{-8})T_r^3] \\ & \times 15{\cdot}4(4{\cdot}4 + 23w_C + 1{\cdot}3w_{Si} \\ & + 0{\cdot}24w_{Cr} + 0{\cdot}94w_{Mo} + 32w_{Ni}) \quad . \; . \; . \quad (10)\end{aligned}$$

where $T_r = T - 25$, T is the transformation temperature in °C, and w represents the concentration of the element identified by the subscript in wt-%. The carbon content used in the calculation was x_γ, the carbon content in the austenite at the start of austempering determined from the austenite–graphite equilibrium at the austenitising temperature. For the alloy described above, this results in a contribution to the strength from austenite of 267 MPa.

GRAPHITE

The yield strength of pure graphite is very dependent on its density, and a variety of values are available in the literature. Therefore, in the present work a value of 120 MPa was used, derived from microhardness measurements and experimentally determined density values.

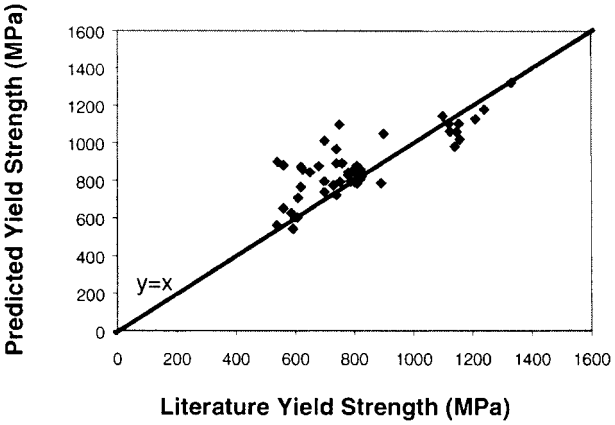

11 Comparison of predicted yield strength and experimental values reported in literature for variety of austempered ductile iron compositions and austenitising and austempering temperatures and times

OVERALL STRENGTH CALCULATIONS

Using the combined microstructural model to calculate the volume fractions of the various phases present and the above expressions for the strength of each of the respective phases, predictions could be made of the overall yield strength as a function of the heat treatment for a particular ADI. To test these predictions, a large database was compiled from information in the literature for over 200 different austempered ductile irons. The information in the database included alloy composition, austenitising and austempering temperatures and times, and any volume fraction and mechanical property information reported in individual papers. Care was taken to extract data at the point corresponding to the end of stage I of the austempering process for which the mechanical properties would be optimum, and therefore direct comparisons could be made with the predictions of the microstructural model.

Figure 11 demonstrates that this simple approach is able to predict the yield strength of different alloys relatively well. There is some degree of overestimation of the yield strength for the lower end of the strength range, probably owing to small errors in the prediction of the volume fraction of bainitic ferrite, and some underestimation at the higher strength region, possibly owing to the neglect of carbide formation within the microstructure. Figure 12 shows the relationship between predicted yield strength and experimental ultimate tensile strength for a number of different austempered ductile irons, from information contained in the database. It can be seen that there is good correlation between the two as expected, and therefore that the predictions of yield strength could be extended to predict ultimate tensile strength; similar relationships can also be determined for hardness. However, prediction of ductility, fatigue, and toughness are likely to demonstrate a more complex dependence on the microstructural constituents than the simpler relationships demonstrated for yield strength and hardness.

Conclusions

A combination of equilibrium thermodynamics and kinetic theory has been used successfully to predict the amounts of the major phases, austenite, graphite, bainite, and martensite, which occur in austempered ductile iron as a function

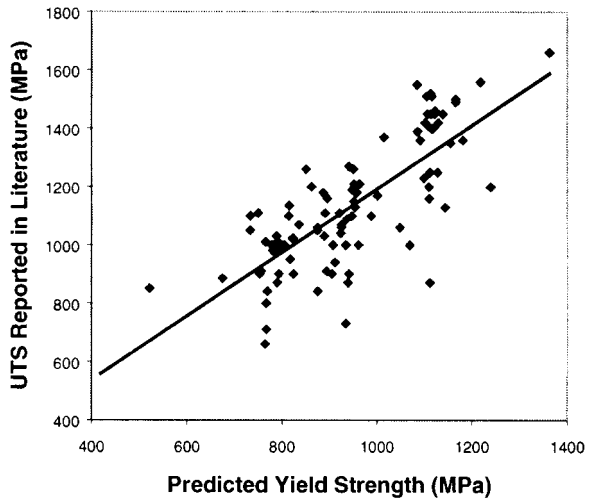

12 Graph illustrating correlation between predicted yield strengths as function of ultimate tensile strengths (UTSs) for variety of austempered ductile iron compositions and austenitising and austempering temperatures and times reported in literature

of heat treatment time and temperature. The inherent segregation present in the microstructure has also been considered using a Scheil approach, which enables predictions to be made of the microstructural constituents as a function of position relative to graphite nodules. A simple law of mixtures model has also been developed to link the microstructural predictions to calculation of mechanical properties; yield strength, ultimate tensile strength, and hardness can be estimated with confidence. Other nonlinear summation methods, models for composite materials, or techniques such as neural network analysis should also be investigated.

A number of assumptions have been made in the present work; in particular there is no treatment of carbide formation, either accompanying the formation of bainite in the stage I reaction or during decomposition of high carbon austenite to ferrite and carbide in the stage II reaction. Therefore, predictions are most useful during stage I of the austempering process. Cooling from austenitising to austempering has been assumed to be rapid enough not to produce other phases within the microstructure, and the complex distribution of phases within actual microstructures has been greatly simplified. These issues will be addressed in future research. Nevertheless, the modelling methodology described in the present work already provides a powerful tool to allow manufacturers of austempered ductile iron to produce the desired properties in particular components, with a significantly reduced number of experimental trials being necessary.

Acknowledgements

The authors would like to thank Federal–Mogul Technology for providing financial support for this project. Fruitful discussions with Professor H. K. D. H. Bhadeshia and support from staff in the Metallurgical Thermochemistry section of the National Physical Laboratory are gratefully acknowledged.

References

1. T. N. ROUNS and K. B. RUNDMAN: *AFS Trans.*, 1987, **95**, 851–874.
2. N. DARWISH and R. ELLIOTT: *Mater. Sci. Technol.*, 1993, **9**, 572–585.
3. H. K. D. H. BHADESHIA: *Mater. Sci. Eng. A*, 1999, **A275**, 58–66.
4. R. H. DAVIES, A. T. DINSDALE, T. G. CHART, T. I. BARRY, and M. H. RAND: *High Temp. Sci.*, 1989, **6**, 251–262.
5. J. S. JAMES: PhD thesis, Loughborough University, UK, 2000.
6. K. W. SOON: MSc thesis, Loughborough University, UK, 1996.
7. G. I. REES and H. K. D. H. BHADESHIA: *Mater. Sci. Technol.*, 1992, **8**, 985–993.
8. N. CHESTER and H. K. D. H. BHADESHIA: *J. Phys. (France) IV*, 1997, **7**, C5, 41–46.
9. H. K. D. H. BHADESHIA: 'Bainite in steels'; 1992, London, Institute of Materials.
10. M. N. AHMADABADI: *Metall. Mater. Trans. A*, 1997, **28A**, 2159–2162.
11. S. J. MATAS and R. F. HEHEMANN: *Trans. AIME*, 1961, **221**, 179–185.
12. M. HILLERT: *Metall. Mater. Trans. A*, 1994, **25A**, 1957–1966.
13. H. K. D. H. BHADESHIA: *Met. Sci.*, 1982, **16**, 167–169.
14. J. S. JAMES and R. C. THOMSON: Proc. Conf. Solid–Solid Phase Transformations 99 (JIMIC-3), Kyoto, Japan, May 1999, Japan Institute of Metals, 1473–1476.
15. R. A. HARDING and N. J. SAUNDERS: Proc. 93rd Annual Conf. of The Institute of British Foundrymen, UK, July 1996, Blackrod.
16. C. F. YEUNG, H. ZHAO, and W. B. LEE: *Mater. Charact.*, 1998, **40**, 201–208.
17. A. S. HAMID ALI and R. ELLIOTT: *Mater. Sci. Technol.*, 1996, **12**, 679–690.
18. M. N. AHMADABADI, E. NIYAMA, and T. OHIDE: *Trans. Am. Foundrymen's Soc.*, 1994, **102**, 269–278.
19. L. NASTAC and D. M. STEFANESCU: *Trans. Am. Foundrymen's Soc.*, 1993, **101**, 933–938.
20. J. LUI and R. ELLIOTT: *Int. J. Cast Metals Res.*, 1998, **10**, 301.
21. J. LUI and R. ELLIOTT: *Int. J. Cast Metals Res.*, 1999, **12**, 75–82.
22. S. YAZDANI and R. ELLIOTT: *Mater. Sci. Technol.*, 1999, **15**, 531–540.
23. S. YAZDANI and R. ELLIOTT: *Mater. Sci. Technol.*, 1999, **15**, 541–546.
24. S. YAZDANI and R. ELLIOTT: *Mater. Sci. Technol.*, 1999, **15**, 888–895.
25. S. YAZDANI and R. ELLIOTT: *Mater. Sci. Technol.*, 1999, **15**, 896–902.
26. K. W. ANDREWS: *J. Iron Steel Inst.*, 1965, **203**, 721–727.
27. R. W. K. HONEYCOMBE and H. K. D. H. BHADESHIA: 'Steels: microstructure and properties', 2nd edn, 1995, London, Edward Arnold.
28. C. H. YOUNG and H. K. D. H. BHADESHIA: *Mater. Sci. Technol.*, 1994, **10**, 209–214.
29. W. C. LESLIE: *Metall. Trans.*, 1972, **3**, 5–26.
30. G. R. SPEICH and H. WARLIMONT: *J. Iron Steel Inst.*, 1968, **206**, 385–392.
31. P. G. WINCHELL and M. COHEN: *Trans. ASM*, 1962, **55**, 347–361.
32. M. TAKAHASHI and H. K. D. H. BHADESHIA: *Mater. Sci. Technol.*, 1990, **6**, 592–603.
33. S. B. SINGH and H. K. D. H. BHADESHIA: *Mater. Sci. Eng. A*, 1998, **A245**, 72–79.